Inorganic Chemistry
Article

Inorg. Chem. **2010**, *49*, 6461–6467 **6461**
DOI: 10.1021/ic100125v

$Ag_6Mo_2O_7F_3Cl$: A New Silver Cathode Material for Enhanced ICD Primary Lithium Batteries

F. Sauvage, V. Bodenez,† J.-M. Tarascon,† and K. R. Poeppelmeier*

Department of Chemistry, Northwestern University, Evanston, Illinois 60208-3113. †LRCS, UMR CNRS 6007, Université de Picardie Jules Verne, 33 rue St. Leu, 80039 CEDEX, France

Received January 20, 2010

As a potential cathode material for the ICD lithium battery, one advantage of $Ag_6Mo_2O_7F_3Cl$ (SMOFC) is its enhanced gravimetric capacity of *ca.* 133 mAh/g above 3 V (vs Li^+/Li) delivered by two biphasic transitions at 3.46 and 3.39 V (vs Li^+/Li). The unique crystal structure of SMOFC enables a high silver ion conduction: $\sigma_{\perp[001]} = 3.10^{-2}$ S/cm ($\pm 2.10^{-2}$ S/cm) and $\sigma_{//[001]} = 4.10^{-3}$ S/cm ($\pm 2.10^{-3}$ S/cm) and, hence, an excellent discharge rate capability. Lithium insertion has been monitored by *in situ* XRD measurements with HRTEM investigations. There is a linear isotropic collapse of the structure leading to a fully amorphous structure beyond four inserted lithiums.

Introduction

Implantable cardioverter defibrillators (ICDs) are medical devices that detect ventricular fibrillation and correct it by administering an electrical shock to the right ventricle.[1,2] $Ag_2V_4O_{11}$ (SVO) was the first practical cathode material proposed back in the 1980s.[3] Since that time, SVO has undergone extensive optimization to enhance its electrochemical reactivity versus lithium either by investigating alternate synthetic strategies[2−7] or by modifying the SVO/electrolyte interface properties.[8,9] At the present time, SVO delivers an optimal gravimetric capacity of about 100 mAh/g (i.e., 480 mAh/cm^3) above 3 V under high pulsed discharge rates. Further improvement of these batteries can be expected only if new cathode candidates are developed with good carrier transport and larger gravimetric/volumetric capacity, in particular above 3 V, combined with chemical and electrochemical stability. With this purpose in mind, our research effort has focused on the synthesis of new silver transition metal oxides for which the oxygen is partially replaced by fluorine to generate new crystal structures that strengthen the ionic character of the 4d (Ag)/2p (O/F) bonds. The $Ag_2O/V_2O_5/HF_{(aq)}$ ternary system was investigated from 150 to 210 °C under hydrothermal conditions and reaction conditions were established that led to the formation of the various known silver vanadates ($Ag_2V_4O_{11}$, β-$AgVO_3$, $Ag_4V_2O_7$, and α-Ag_3VO_4) and more interestingly to the first silver dense vanadium oxyfluoride, $Ag_4V_2O_6F_2$ (SVOF; ρ = 6.03 g/cm^3).[10−12] Its electrochemical reactivity with respect to lithium metal was appealing with a superior capacity above 3 V of *ca.* 148 mAh/g (i.e., 892 mAh/cm^3) provided by exclusive Ag^+/Li^+ displacement reactions at 3.45 and 3.35 V (vs Li^+/Li).[13] In this work, we investigate the electrochemical properties of another compound with a high density of silver, $Ag_6Mo_2O_7F_3Cl$ (SMOFC).[14] An additional advantage compared to SVO/SVOF or SMOF ($Ag_3MoO_3F_3$[15]) is its larger tunnels which favor the kinetics for the Ag^+/Li^+ displacement reaction. The lithium insertion properties of $Ag_6Mo_2O_7F_3Cl$ (SMOFC) are explored in this manuscript, and the mechanism is discussed on the basis of *in situ* XRD experiments and HRTEM observations. The potential advantage of SMOFC compared to SVOF and SVO will also be discussed on the basis of differences in their electrochemistry.

*To whom correspondence should be addressed. E-mail: krp@northwestern.edu.

(1) Skarstad, P. M. *J. Power Sources* **2004**, *136*, 263–267.
(2) Crespi, A. M.; Somdahl, S. K.; Schmidt, C. L.; Skarstad, P. M. *J. Power Sources* **2001**, *96*, 33–38.
(3) Takeuchi, K. J.; Marschilok, A. C.; Davis, S. M.; Leising, R. A.; Takeuchi, E. S. *Coord. Chem. Rev.* **2001**, *219*, 283–310.
(4) Sauvage, F.; Bodenez, V.; Vezin, H.; Morcrette, M.; Tarascon, J.-M.; Poeppelmeier, K. R. *J. Power Sources* **2010**, *195*, 1195–1201.
(5) Zhang, S.; Li, W.; Li, C.; Chen, J. *J. Phys. Chem. B* **2006**, *110*, 24855–24863.
(6) Beninati, S.; Fantuzzi, M.; Mastragostino, M.; Soavi, F. *J. Power Sources* **2006**, *157*, 483–487.
(7) Takeuchi, K. J.; Marschilok, C. A.; Leising, R. A.; Takeuchi, E. S. *MRS Symp. Proc.* **2007**, *972*, 351–356.
(8) Lee, J.-W.; Popov, B. N. *J. Power Sources* **2006**, *161*, 565–572.
(9) Leising, R.A.; Takeuchi, E.S. U.S. Patent: US2003138697.
(10) Sorensen, E. M.; Izumi, H. K.; Vaughey, J. T.; Stern, C. L.; Poeppelmeier, K. R. *J. Am. Chem. Soc.* **2005**, *127*, 6347–6352.
(11) Izumi, H. K.; Sorensen, E. M.; Vaughey, J. T.; Poeppelmeier, K. R. U.S. Provisional Patent 60/606, 475, Sept. 1, 2004.
(12) Albrecht, T. A.; Stern, C. L.; Poeppelmeier, K. R. *Inorg. Chem.* **2007**, *46*, 1704–1708.
(13) Sauvage, F.; Bodenez, V.; Vezin, H.; Albrecht, T. A.; Tarascon, J.-M.; Poeppelmeier, K. R. *Inorg. Chem.* **2008**, *47*(19), 8464–8472.
(14) Maggard, P. A.; Nault, T. S.; Stern, C. L.; Poeppelmeier, K. R. *J. Solid State Chem.* **2003**, *175*, 27–33.
(15) Tong, W.; Yoon, W. S.; Hagh, N. M.; Amatucci, G. G. *Chem. Mater.* **2009**, *21*, 2139.

Published on Web 06/14/2010

Table 1. Synthesis Conditions for the Preparation of $Ag_6Mo_2O_7F_3Cl$ Single Crystals

	Ag_2O	MoO_3	4OH−pyr.	HF_{aq} (48−50%)	HCl (37%)	H_2O
ratio	3	2	1	40	0.75	0 or 7.50
moles	3.33×10^{-3}	2.22×10^{-3}	1.11×10^{-3}	2.22×10^{-2}	8.325×10^{-4}	0 or 8.33×10^{-3}
mass	0.773 g	0.32 g	0.107 g	0.788 g	0.013 g	0 or 0.15 g

Table 2. Synthesis Conditions for the Preparation of Polycrystalline $Ag_6Mo_2O_7F_3Cl$

	Ag_2O	MoO_3	4OH−pyr.	HF_{aq} (48−50%)	HCl (37%)	H_2O
ratio	2	2	5	30	4	4
moles	2.22×10^{-3}	2.22×10^{-3}	5.55×10^{-3}	2.22×10^{-2}	4.44×10^{-3}	8.33×10^{-3}
mass	0.515 g	0.32 g	0.535 g	0.591 g	0.069 g	0.15 g

Experimental Section

$Ag_6Mo_2O_7F_3Cl$ (SMOFC) Synthesis Procedure. $Ag_6Mo_2O_7F_3Cl$ was synthesized by a hydro(-solvo-)thermal method in self-contained FEP Teflon pouches using three different preparation routes. The reagents used include Ag_2O, MoO_3, 4-hydroxypyridine, $HF_{(aq)}$ (48−50%), and $HCl_{(aq)}$ (37%). 4-hydroxypyridine prevents AgCl precipitation following the addition of $HCl_{(aq)}$.

The first two preparation routes (see Table 1) use the same ratio of Ag/Mo/4-hydroxypyridine/HF/HCl (3:2:1:40:0.75). As listed in the last column, the difference lies in the supplementary addition of water, which led to improved reproducibility in obtaining clear transparent single crystals. The yield was 20% based on silver.

The third route involves a different molar ratio of the reactants (see Table 2). This procedure yields light gray polycrystalline SMOFC particles and increases the yield to 72%.

Regardless of the synthetic procedure followed, the pouches with reactants were heat sealed and subsequently placed inside a 125 mL PTFE Teflon liner backfilled with 42 mL of deionized H_2O. The autoclave was heated to 150 °C for 24 h and then slowly cooled at 0.1 °C/min to room temperature. The product was retrieved by vacuum filtration and thoroughly rinsed with water.

$Ag_4V_2O_6F_2$ (SVOF) and $Ag_2V_4O_{11}$ (SVO) Synthesis Procedure. $Ag_4V_2O_6F_2$ was prepared as reported previously[11,13] with a 4:1:30 molar ratio of Ag_2O, V_2O_5, and $HF_{(aq)}$. Red and transparent needle-like single crystals of SVOF were recovered by vacuum filtration in around 40% yield based on Ag.

$Ag_2V_4O_{11}$ was synthesized similarly to the hydrothermal procedure used to synthesize SVOF at 150 °C for 24 h. A 1:2.5:35 molar ratio of Ag_2O, V_2O_5, and $HF_{(aq)}$ produces pure SVO in 60% yield (referenced hereafter as SVO-HT).

Physical Characterization. The X-ray powder diffraction (XRD) patterns were recorded in a ($\theta/2\theta$) configuration using a Bruker D8 diffractometer with Cu K_α radiation (λ = 0.15418 nm). The particle size and morphology were investigated using an FEI Quanta 200FEG environmental scanning electron microscope (ESEM) coupled with an energy dispersion spectroscopy (EDS) analysis system (Oxford Link Isis). *In situ* XRD experiments were performed using a specific electrochemical cell capped by a Be window as a current collector. A Mac Pile galvanostat was used to control the cell discharge to a D/10 rate corresponding to the insertion of one lithium in 10 h. The XRD patterns were collected at intervals of 0.125 Li^+ inserted. High resolution transmission electron microscopy observations on discharged particles were carried out using an FEI TECNAI F20S-twin. For this, the discharged battery was dismantled in an Ar-filled glovebox, and the retrieved cathode material was thoroughly washed three times in dimethyl carbonate (DMC) before being deposited on a copper grid coated with a holey-carbon film. A specific TEM sample holder, which allows the investigation of air-sensitive materials, was used to prevent the discharged material from reacting with air before the microscope observations.

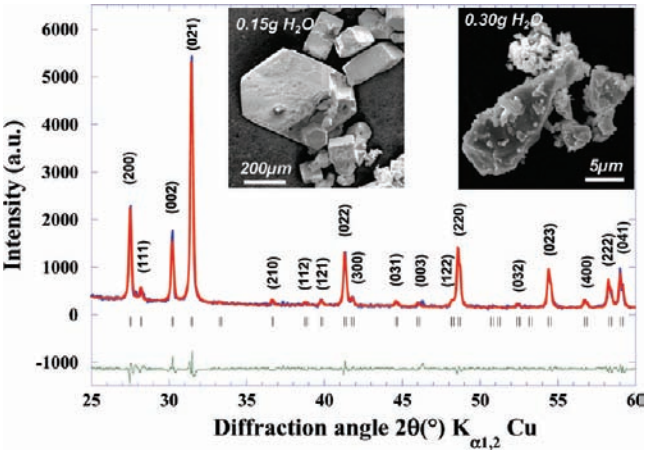

Figure 1. Full-pattern matching refinement of the X-ray diffraction pattern collected on the pristine $Ag_6Mo_2O_7F_3Cl$ (SMOFC) obtained using the second route with 0.15 g of H_2O. In the inset, SEM pictures of the hexagonal single crystal and the smaller particles synthesized by adding 0.15 and 0.30 g of water, respectively.

Electrochemical Tests. The electrochemical characterization of SMOFC was carried out by manually grinding for 30 min the active material together with SP-type carbon black in a proportion of 14% by weight. The two-electrode measurements were performed using Swagelok-type cells assembled in an Ar-filled drybox. A lithium metal foil was used both as a counter and a reference electrode. Two pieces of a Whatman GF/D borosilicate glass fiber sheet separator were thoroughly soaked with 1 M $LiPF_6$ EC/DMC 1:1 electrolyte (LP30 − Merck Selectipur grade). The cells were monitored by a VMP multipotentiostat (Biologic SA, Claix, France).

Results and Discussion

Figure 1 shows the refined X-ray diffractogram, using Fullprof software in the full-pattern matching mode, of the recovered product obtained from the second synthetic route. All of the reflections collected are indexed in the trigonal *P*3*m*1 space group (no. 156). The refined lattice cell parameters are a = 7.489(1) Å and c = 5.917(1) Å. The insets are SEM images of crystallites prepared with the addition of 0.15 and 0.30 g of H_2O, respectively. The decrease of the precursor's concentration by adding an extra amount of water to the pouch (0.15 g vs 0.30 g H_2O) noticeably affects the nucleation and growth processes, which leads to a decrease in crystallite size. Note that, for a lower reagent concentration (*e.g.*, 0.30 g of additional water), the hexagonal shape of the crystals vanishes and the yield based on Ag decreases to ∼10%. The synthesis of SMOFC as a single phase without extra water was more complicated to control since the presence of an additional unidentified beige product was sometimes

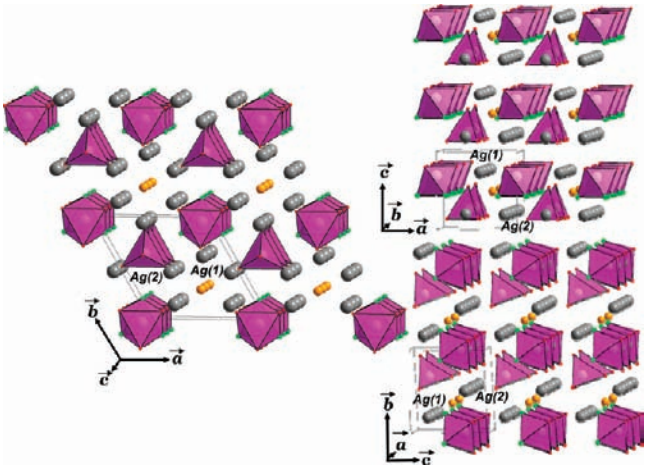

Figure 2. Crystal structure representation of SMOFC in the *ab*, *ac*, and *bc* planes with the Mo^{6+}-centered polyhedron.

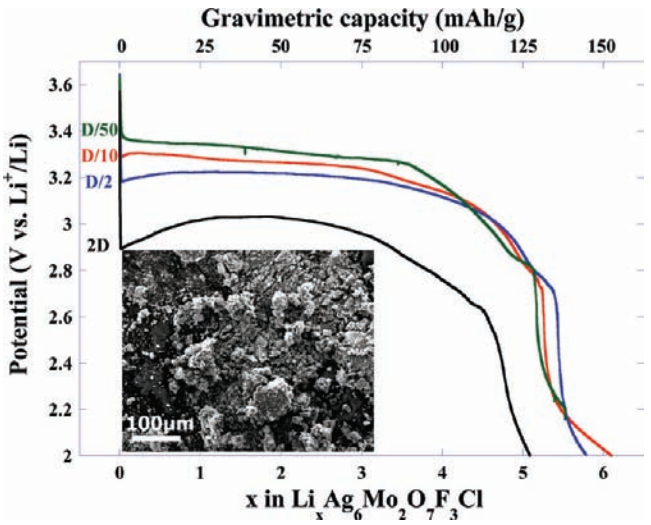

Figure 3. Influence of the discharge rate from D/50 to 2D on the electrochemical discharge traces of a composite SMOFC/C_{sp} electrode in a 1 M $LiPF_6$ EC/DMC 1:1 electrolyte down to a 2 V cutoff voltage. In the inset are scanning electron microscopy pictures of manually ground SMOFC single crystals with 14 wt % C_{sp}.

observed. The SEM micrographs show that, at higher reagent concentrations, hexagonal single crystals (~0.5 mm) were recovered. The second SEM micrograph highlights the morphological loss and the particle size decrease to ~10 μm driven by the addition of 0.30 g of H_2O into the pouch.

The crystal structure of SMOFC is comprised of isolated $[MoO_3F_3]^{3-}$ octahedra and $[MoO_4]^{2-}$ tetrahedra (Figure 2). SMOFC's structure contains two crystallographically distinct types of Ag^+ cations. As seen in Figure 2b and c, Ag(1) and Ag(2) lie in separate layers with Ag(1) alternating with $[MoO_3F_3]^{3-}$ octahedral units and Ag(2) with $[MoO_4]^{2-}$ units. While the disconnected character of the Mo polyhedron is likely detrimental for high electronic conduction, it provides multiple pathways for Li^+ and Ag^+ ion conduction.

Electrochemical investigations have been performed on ground fresh single crystals (synthetic procedure 1). This step mills the single crystals into particles of heterogeneous size ranging from 10 to 50 μm (Figure 3, inset). The discharge curve (Figure 3) operated at D/50 (*i.e.*, one lithium inserted in 50 h) traces two close composition-potential plateaus centered

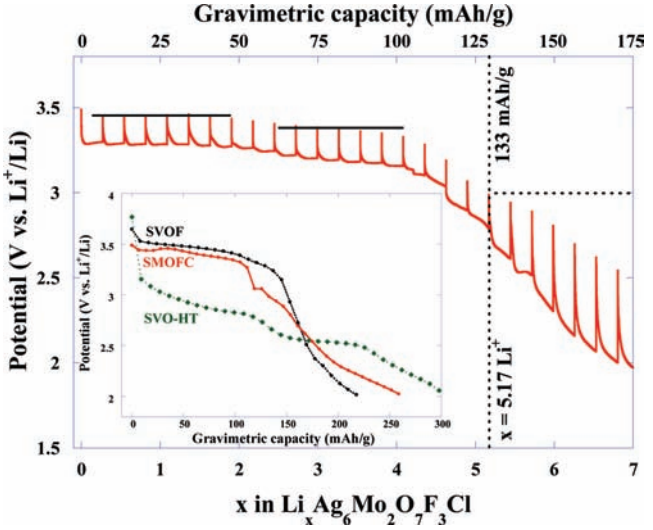

Figure 4. GITT discharge curve of the SMOFC/C_{sp} composite electrode in a 1 M $LiPF_6$ EC/DMC 1:1 electrolyte (D/10 discharge rate for 2 h followed by 15 h relaxation time). In the inset is a comparison of the discharge trace at equilibrium for SMOFC, SVOF, and SVO-HT.

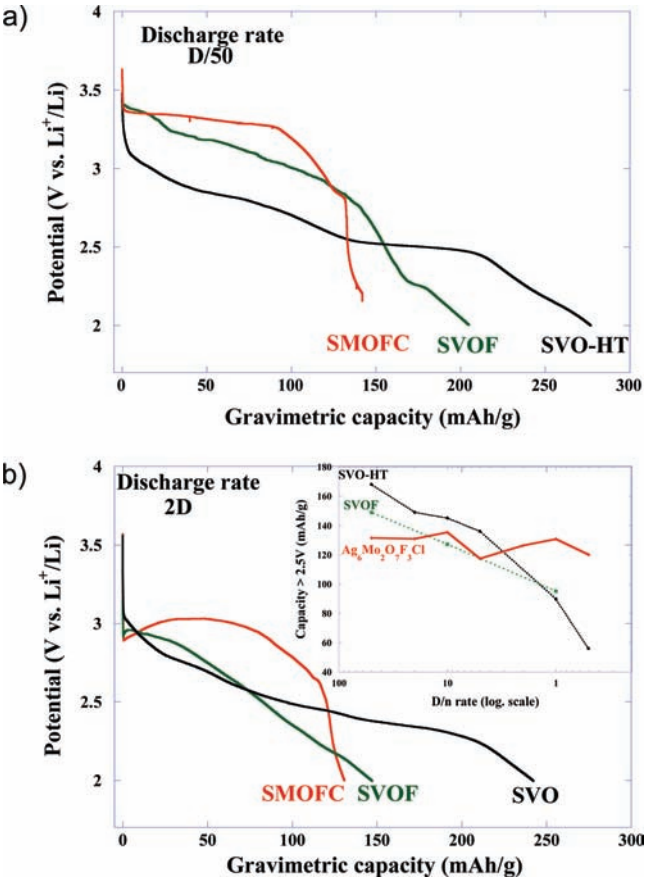

Figure 5. Galvanostatic-driven discharge comparison between SMOFC, SVOF, and SVO-HT performed at (a) D/50 and (b) 2D (rate discharge capability curve above 2.50 V in inset).

between 3.40 and 3.30 V (vs Li^+/Li) over the course of the insertion of around 4 Li^+ per formula unit. The insertion of two additional Li^+'s is accompanied by a drop to 2 V. The gravimetric capacity of SMOFC is about 150 mAh/g, which corresponds to a theoretical volumetric capacity of 913 mAh/cm^3

($\rho_{(SMOFC)}$ = 6.09 g/cm^3). Interestingly, the amount of lithium inserted matches the silver stoichiometry of SMOFC. When increasing the discharge rate from D/50 to 2D, the cathode maintains a moderate polarization increase over the two plateaus that does not radically affect the capacity above 2 V (i.e., 5 Li^+ can still be inserted). A galvanostatic intermittent titration technique (GITT) experiment was carried out to better quantify this electrode overpotential and also to give insight on the mechanism for Li^+ insertion. For this, a discharge rate condition of D/10 was applied for 2 h, corresponding to the insertion of 0.2 Li^+. This was followed by a relaxation stage of 15 h to allow the material to recover to its equilibrium state (Figure 4). The GITT curve better resolves the features of the two voltage-composition plateaus at 3.46 and 3.39 V (vs Li^+/Li). Each plateau involves the insertion of approximately the same amount of lithium. Despite the large size of the particles (~10−50 μm), the overpotential, defined here as the potential difference between the OCV curve and the one under current, is around 170 mV. This value is significantly lower than the barrier of 400 mV required for SVOF particles of similar size.[13] After 5 Li^+'s are inserted, the aforementioned potential drop is accompanied by a significant overpotential increase, indicative of kinetic impediments to further lithium insertion. Above 3 V, SMOFC provides a gravimetric capacity of 133 mAh/g, which corresponds to around 5.2 Li^+'s inserted per formula unit. Note that the smaller size of the particle produced by route 3 provides similar performances even at a 2D discharge rate (see Supporting Information Figure S1).

SMOFC's conductivity was evaluated by AC measurements using Pt blocking electrodes parallel and perpendicular to the [001] direction of the single crystal. The impedance response is indicative of silver ion blocking at low frequencies. Interestingly, SMOFC exhibits high conductivity, $\sigma_{//[001]} = 3.10^{-2}$ S/cm ($\pm 2.10^{-2}$ S/cm) and $\sigma_{(110)} = 4.10^{-3}$ S/cm ($\pm 2.10^{-3}$ S/cm) (*n.b.*, error bars were evaluated by repeating the measurements on

Table 3. Capacity Comparison Recorded at a 2D Discharge Rate between $Ag_6Mo_2O_7F_3Cl$ (SMOFC), $Ag_4V_2O_6F_2$ (SVOF) Synthesized under Hydrothermal Conditions, and $Ag_2V_4O_{11}$ (SVO) Prepared by Hydrothermal Synthesis

	SMOFC		SVOF		SVO (HT)	
ρ (g/cm^3)	6.09		6.03		4.80	
	mAh/g	mAh/cm^3	mAh/g	mAh/cm^3	mAh/g	mAh/cm^3
capacity > 3 V	65.7	399.5	0	0	1	4.8
capacity > 2.5 V	120.1	731.5	82.5	497.5	60.4	289.9
capacity > 2 V	130.7	796	146.7	884.6	218.8	1050

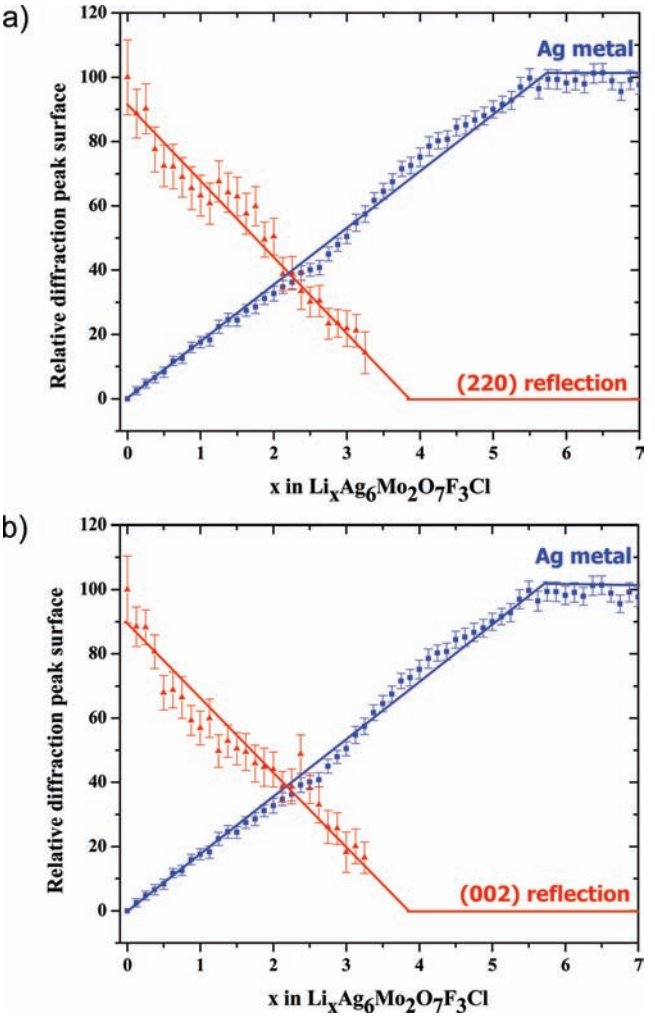

Figure 7. Evolution of the silver metal and SMOFC XRD peak area as a function of x in Li_xSMOFC for the directions (a) (220) and (b) (002).

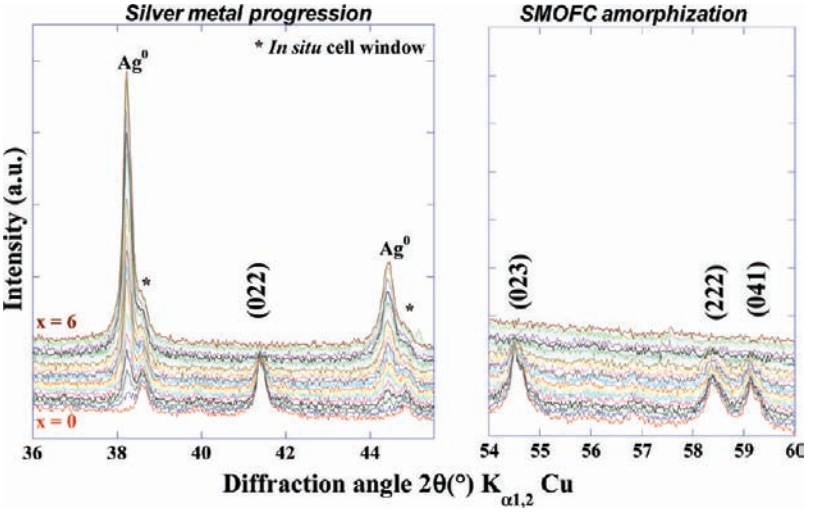

Figure 6. *In situ* evolution of the XRD pattern recorded after every 0.25 Li^+ was inserted at a D/10 discharge rate between Li_0-SMOFC and Li_6−SMOFC in a 2θ range of (a) 36−45° showing the silver appearance and (b) 54−60° showing SMOFC amorphization.

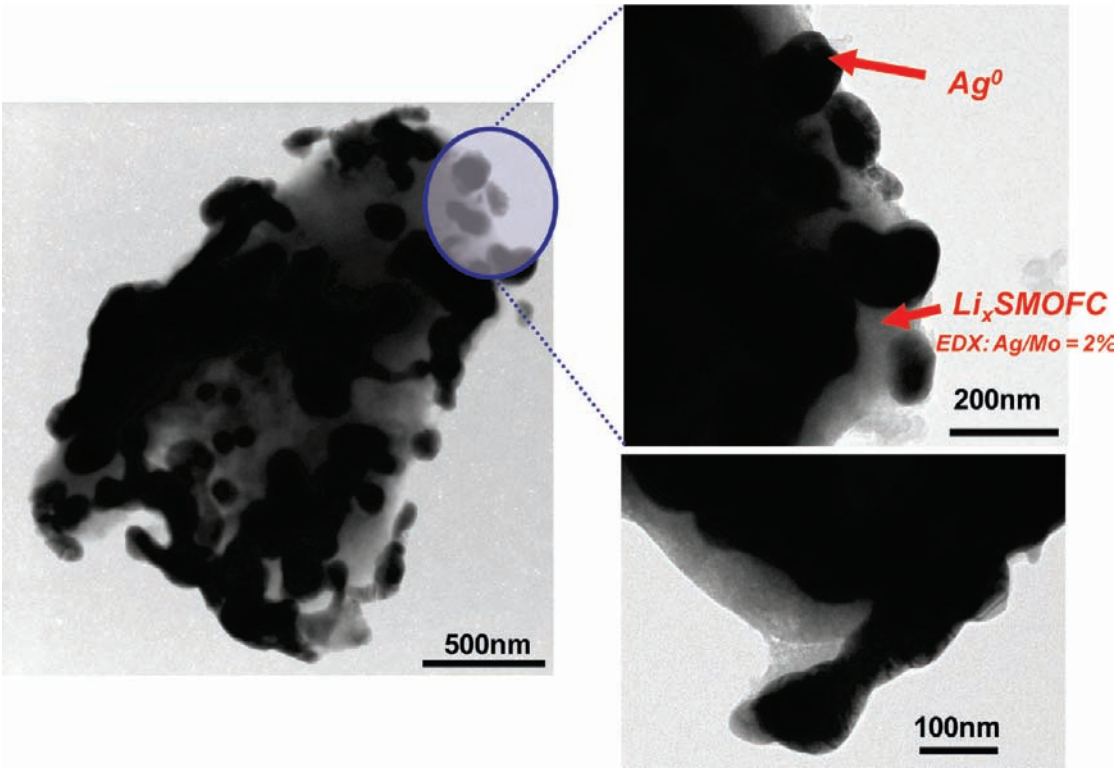

Figure 8. High resolution transmission electron microscopy bright field image obtained on an electrochemically discharged Li_6SMOFC.

different single crystals), with an ionic conductivity greater by 1 order of magnitude along the [001] direction. This excellent conduction of the silver ion, which results from SMOFC's peculiar structure, is comparable with the best silver glass conductors, such as those within the $AgI-Ag_2MO_4$ (M = W, Mo) system.[16,17] The high discharge rate capability of SMOFC related to the lower polarization can thus be explained on the basis of this high ionic conductivity. Nevertheless, this high silver transport is also a potential culprit for the decomposition of SMOFC into AgCl, Ag^0, and an unidentified phase upon exposure to ambient light over a period of two months.

The electrochemical performance of SMOFC vs lithium was compared to those of SVOF and SVO-HT following the same electrochemical and electrode formation procedure. In this comparative survey, SVOF and SMOFC display similar particle sizes;[13] however, particles of SVO-HT adopt a flat needle-like morphology of a few micrometers-long, 200−500-nm-wide, and 100-nm-thick.[4] For this reason, care is required not to over interpret such comparisons owing to morphology, size, and porosity variations between the various electrode materials. Owing to the presence of Ag^+ and the ability of V^{5+} to reduce to V^{4+}, SVO provides the greatest gravimetric capacity above 2 V at D/50 as well as at 2D (Figure 5). In contrast, the oxyfluorides deliver at higher voltage for the first 150 mAh/g (Figure 4, inset). This difference, which reaches 500−600 mV at D/50, would therefore greatly improve the power delivery of the battery (Figure 5a). At a faster discharge rate (2D), the oxyfluorides perform closer to the benchmark SVO cathode. A lower capacity discrepancy between SVOF and SMOFC beyond 2 V is experienced as a result of the high discharge rate capability of SMOFC. It delivers at 400 mV greater than SVO when using this stringent discharge condition (Figure 5b). Furthermore, owing to their higher silver content (6.0 g/cm^3 vs 4.80 g/cm^3 for SVO), the oxyfluorides hold a significant advantage in terms of crystal structure density, which would greatly impact the volumetric power of the battery pack. All of these results are summarized in Table 3 for three different cutoff potentials (3, 2.5, and 2 V).

In situ XRD measurements during discharge and HRTEM on the discharged cathode were used as a complementary set of techniques to probe the lithium insertion mechanism in SMOFC and scrutinize the effects of inserting lithium on the host structure. Figure 6 gathers the diffractograms collected from $x = 0-6$ in Li_xSMOFC. At the onset of the discharge, two diffraction peaks centered at 38.2° and 44.4°, assigned to silver metal, progressively increase in intensity. This progression comes concomitantly with a decrease in the peak intensities associated with SMOFC, without any shift of their position, consistent with a biphasic transition. The progress of the silver reduction and the amorphization of the host Li_x−SMOFC structure were probed by integrating the area under the silver metal and Li_x−SMOFC diffraction peaks. A linear evolution of the silver metal's peak area as a function of the amount of lithium inserted is observed until a maximum is reached at approximately $x = 6$ (Figure 7). Interestingly, the same integration procedure for the (220) and (002) reflection of the host structure also shows a linear dependence with lithium leading to an XRD featureless structure after $x = 3.8$ Li^+ is inserted. This linear decrease and subsequent disappearance of SMOFC diffraction peaks was also noted in the (200), (021), and (022) directions. This result suggests an isotropic collapse of the structure, resulting from the numerous pathways for the Ag^+ withdrawal from the structure. This collapse is driven by the significant ionic radii mismatch between Li^+ and Ag^+ ($r_{(Li+)} = 0.76$ Å and $r_{(Ag+)} = 1.15-1.35$ Å). This is

(16) Kuwano, J.; Kato, M. *Dengi Kagaku* **1978**, *46*, 353.
(17) Hosono, M.; Kawamura, J.; Itoigawa, H.; Kuwata, N.; Kamiyama, T.; Nakamura, Y. *J. Non-Cryst. Solids* **1999**, *244*, 81–88.

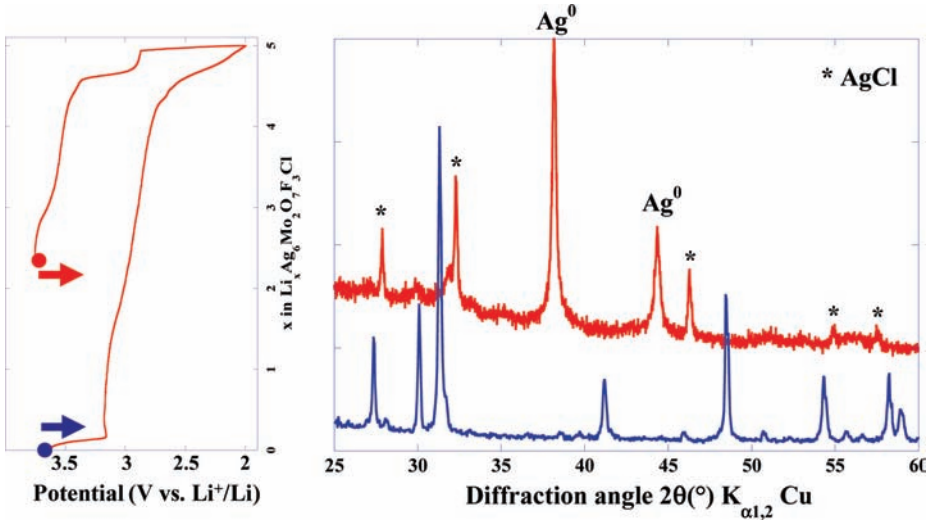

Figure 9. Galvanostatic curve recorded at C/10 showing the reversibility of the Ag^+/Li^+ displacement reaction in SMOFC with the XRD pattern collected at the initial stage of the discharge and at the end of the recharge.

also to a lesser extent promoted by the increase in electrostatic repulsion between the $[MoO_4^{2-}]$ and $[MoO_3F_3^{3-}]$ polyhedra when Ag^+ is replaced by Li^+.[18]

Further information on the local structure of Li_6−SMOFC, electrochemically discharged at a D rate, was obtained from HRTEM observations. The bright field image in Figure 8 shows the coexistence of two contrasts within the particles. The dark regions arise from the metallic silver that has withdrawn from the crystals, while the bright zone of the particles is assigned to the discharged Li_6−SMOFC. EDX measurements at this location indicate that essentially all of the silver is displaced, giving a Ag/Mo atomic ratio of only 0.02. Furthermore, this region of the particle exhibits an entirely amorphous structure with no signs of nanocrystalline domains. The silver metal is partially wrapped around the discharged particles and adopts the morphology of the particle's edge. In contrast to our previous observation on SVOF samples, neither long silver dendrites nor nanocrystalline silver particles were observed.[13] This behavior of the silver particles (morphology) was not dependent on the discharge rate. The extended percolation of the silver metal network inside the Li_xSMOFC crystallites contributes to multiple electronic conduction pathways. This allows the partial reduction of the molybdenum (+VI) at around 2.5 V; that is associated with a noticeable increase in the electrode polarization of more than 500 mV (Figure 4). Note that below 2 V, the molybdenum reduction competes with the Ag/Li alloying reaction.

Owing to its mixed O/F coordination, Ag(1) is assumed to be reduced before Ag(2) during the first discharge plateau. In contrast to SVOF, the Ag^+/Li^+ displacement reaction was found to be partially reversible (Figure 9). However, the initial structure is not recovered by the oxidation and intake of silver ion. The XRD diffractogram collected on the recharged product suggests that Ag^+ reacts with the Cl^- anions present in the structure to form crystalline AgCl clusters. However, the efficiency of this reaction dramatically diminishes during subsequent cycles. The complete first cycle of SMOFC carried out at a *C* rate is reported in Figure S2 (see the Supporting Information).

(18) Shannon, R. D. *Acta Crystallogr.* **1976**, *A32*, 751.

Conclusion

Following our first reports on the lithium insertion properties of SVOF, we have begun to investigate other dense silver oxyfluoride compounds for which the crystal structure displays larger channels to facilitate the silver displacement reaction and at the same time contains a transition metal element less toxic than vanadium. Our choice turned toward $Ag_6Mo_2O_7F_3Cl$ because it exhibits a unique 3D crystal structure consisting of isolated $[MoO_4^{2-}]$ tetrahedra and $[MoO_3F_3^{3-}]$ octahedra templated around the Cl^- anion. The preliminary study of the lithium insertion in this material highlights very appealing electrochemical behavior. A gravimetric capacity of 133 mAh/g is available above 3 V with an excellent discharge rate capability. The origin of this high discharge rate capability is attributed to the excellent silver ion conduction of $\sigma_{\perp[001]} = 3.10^{-2}$ S/cm ($\pm 2.10^{-2}$ S/cm) and $\sigma_{//[001]} = 4.10^{-3}$ S/cm ($\pm 2.10^{-3}$ S/cm). *In situ* XRD measurements combined with HRTEM investigations suggest an exclusive Ag^+/Li^+ displacement reaction between Li_0Ag_6MOFC and $Li_{\sim 6}Ag_{\sim 0}$MOFC along with a continuous isotropic structure amorphization to $Li_{\sim 3.8}Ag_{\sim 2.2}$MOFC, which is the composition threshold at which the electrode becomes entirely XRD amorphous. This amorphous structure is maintained during the cathode recharge. Interestingly, the recharge, enabling the reincorporation of Ag^+, follows another path by reacting with Cl^- to form polycrystalline AgCl. More in-depth electrochemical investigations will be needed, in particular near operating conditions (37 °C, pulsed discharge current, etc.) to confirm the potential of SMOFC for this application.

Acknowledgment. The authors gratefully acknowledge Dr. T. A. Albrecht for fruitful discussions. This work was supported from the Office of Naval Research (MURI Grant N00014-07-1-0620) and the National Science Foundation (Solid State and Materials Chemistry Award No. DMR-0604454). This work made use of the J. B. Cohen X-Ray Facility supported by the MRSEC program of the National Science Foundation (DMR-0520513) at the Materials Research Center of Northwestern University. Vincent Bodenez is indebted

to the Conseil Regional de Picardie (France) for financial support.

Supporting Information Available: Comparison of the galvanostatic discharge curve recorded at a 2D rate between a SMOFC produced by route 2 and SMOFC particles synthesized by route 3 and the first cycle of SMOFC recorded in galvanostatic mode at a *C* rate (*i.e.*, 1 Li^+ exchanged per hour) between 4 and 0.01 V (vs Li^+/Li) in a 1 M $LiPF_6$ EC/DMC 1:1 electrolyte. This material is available free of charge via the Internet at http://pubs.acs.org.